AC Corrosion and the Pourbaix Diagram

Andreas Junker, M.Sc., Eng.
MetriCorr, Toerringvej 7, 2610 Roedovre Denmark
Technical University of Denmark, Produktionstorvet B425, 2800 Kgs. Lyngby, Denmark

Lars Vendelbo Nielsen, Ph.D., Eng.
MetriCorr, Toerringvej 7, 2610 Roedovre Denmark

Per Møller, Prof., Eng.
Technical University of Denmark, Nils Koppels Allé B404, 2800 Kgs. Lyngby, Denmark

CeoCor Conference
15-18 May, 2018
Stratford-upon-Avon, United Kingdom

AC Corrosion and the Pourbaix Diagram

Andreas Junker, M.Sc., Eng.
MetriCorr, Toerringvej 7, 2610 Roedovre Denmark
Technical University of Denmark, Produktionstorvet B425, 2800 Kgs. Lyngby, Denmark

Lars Vendelbo Nielsen, Ph.D., Eng.
MetriCorr, Toerringvej 7, 2610 Roedovre Denmark

Per Møller, Prof., Eng.
Technical University of Denmark, Nils Koppels Allé B404, 2800 Kgs. Lyngby, Denmark

Abstract

AC interference on cathodically protected pipelines is of major concern due to the risk of AC corrosion. Corrosion is generally linked to AC and DC current densities, but incoherence in data from different researches is often difficult to explain. In this paper, ER-probe corrosion rate data from multiple experiments is used to illustrate how the accepted AC and DC current density criteria may, in fact, be closely linked to thermodynamically calculated Pourbaix diagrams. The concepts are illustrated by simple model experiments and discussed in a theoretical context, based on literature. AC is shown to cause de-alkalisation of steel under galvanostatic cathodic protection, possibly causing low pH corrosion. This discovery may necessitate a critical re-evaluation of literature investigations of AC corrosion under galvanostatic cathodic current.

Introduction

The Pourbaix diagram or potential/pH diagram depicts the electrochemical stability regions of different metal and mineral phases with respect to potential and pH. Once one understands the applicability of these diagrams they are extremely useful for corrosion engineers. Figure 1 shows the Pourbaix diagram for iron calculated at standard conditions (25°C, 1 bar) and the Gibbs free energy, Δ*G*, of the involved substances. The potentials are given with respect to the $Cu/CuSO_4$ electrode (CSE) (shifted -316 mV with respect to the hydrogen electrode).

Substance	Δ*G* (kcal./mol)	Name
Fe	0.000	Iron
Fe_2O_3	-177.114	Hematite
Fe_3O_4	-242.645	Magnetite
$Fe(OH)_2$	-117.464	Ferrous hydroxide
FeOOH	-116.928	Goethite (α)
Fe^{3+}	-4.107	Ferric ion
Fe^{2+}	-21.875	Ferrous ion
$HFeO_2^-$	-95.353	Dihypoferrite ion

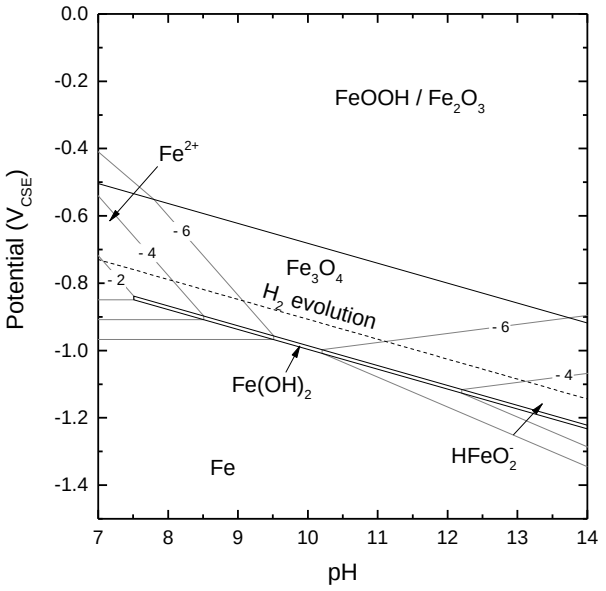

Figure 1: Calculated Pourbaix diagram for iron in neutral to alkaline environment. Varying concentrations (log(mol/L)) of dissolved ions influence the stability regions. Potentials with respect to $Cu/CuSO_4$.

The values of Δ*G* used here differ slightly from those originally used by Pourbaix which explains the larger $HFeO_2^-$ region compared to traditional Pourbaix diagrams (Pourbaix used Δ*G* = -90.627 kcal./mol for the dihypoferrite ion). [1] The listed values are standard values in the HSC Chemistry software used for the calculation. The choice of considered species for drawing the diagram introduces a narrow $Fe(OH)_2$ region below Fe_3O_4, and a region of stability, at higher potentials, being either FeOOH or Fe_2O_3.

To be able to use the Pourbaix diagram and conclude anything about a corrosion process, one needs to be able to determine the necessary potentials and pH. Both have practical challenges:

- Potential measurements will always be an average across local surface potential variations. Even for polarised surfaces.
- For polarised surfaces, the local potential variations may be small, but here, an IR drop needs to be considered, due to the current passing through the electrode/electrolyte interface.
- One can only discuss a potential with respect to a reference potential. Several reference electrodes exist, but they may all suffer from potential drift (for various reasons) and require careful calibration and maintenance.
- Most pH measurements also rely on potential measurement, and thus the same challenges as for potential measurements exist here.
- Potential sensitive pH measurement techniques cannot be performed in the electric field of a polarised surface without introducing an error.
- pH measurement by conventional methods requires a certain measurement volume but the pH gradient towards a cathodically protected surface is very steep, yielding an infinitely small measurement volume for obtaining the true surface pH.

In this study, pH is measured using small pH glass tip electrodes and efforts have been made to minimize the effects of drifting potentials by calibration before and after and compensation of data accordingly. In addition, the electric field from cathodic protection and AC interference was periodically turned off during pH measurements. The biggest challenge with regard to pH measurement faced in this study was the limited measurement volume and the placement of the electrodes.

For comparison with large amounts of data, in which no actual pH measurement was available, the close correlation between the cathodic current density and pH is utilized. [2] Figure 2 shows measured pH as a function of cathodic current density compared to data measured by several other authors (using various techniques). This Figure is a reprint from previous work by Angst *et al.*(2016) with the inclusion of additional data points, especially in the high pH region. [3] [4]

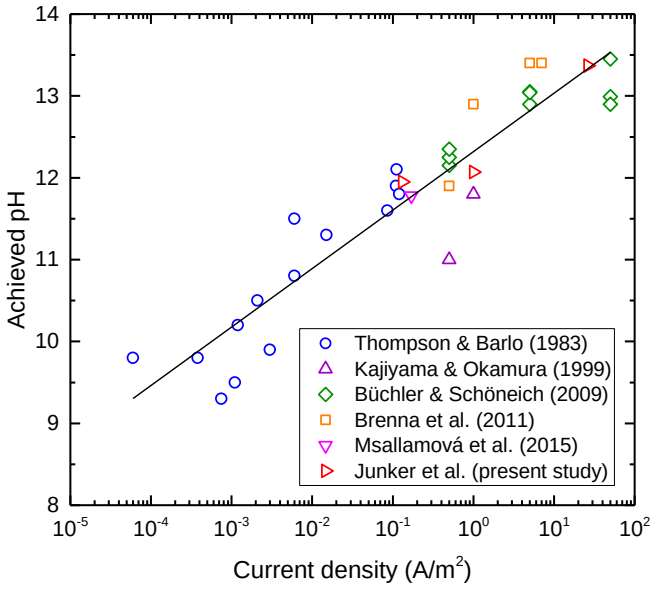

Figure 2: Achieved pH of a steel electrode as a function of the cathodic protection current density. Reprint from [3] with additional data [4]. Full line is a fit of all datapoints.

The line is a fit of all data points with $p = 0.714$ and $pH_0 = 12.318$ in equation (1). This is very similar to the values suggested by Büchler and Joos (2016) ($p = 0.5$ and $pH_0 = 12.4$)with a slightly stronger dependence on $-J_{DC}$ due to the higher p-value. [5]

$$pH = pH_0 + p \cdot \log(-J_{DC}) \quad (1)$$

By using this simple equation, in which the current density is an easily measured parameter, one has a good approximation of the actual surface pH of steel under cathodic protection.

Surface potential measurement is a fundamental part of cathodic protection monitoring. However, it is debated whether, even under cathodic protection, each individual coating defect on an entire pipeline has its own potential, and that the measured pipeline potential is found to follow the potential of larger defects. [6] In laboratory investigations where a single simulated coating defect is investigated, this discussion is of less importance. IR drop compensation to obtain the true surface potential may be achieved by different methods, as outlined below:

- Laboratory investigations often use a Luggin capillary to provide a conductive path, in which no current runs, between the reference electrode and the surface to be measured. This method is obviously impractical for pipeline applications with coating holidays of unknown numbers and locations. Even in laboratory use, the placement of the Luggin capillary becomes important since the majority of the IR drop occurs in very close proximity to the electrode where the current density in the electrolyte is highest.
- On-Off potential measurements, in which the polarisation current is momentarily disrupted, are routinely used to determine a pipeline's *polarised* or *instant-off* potential. This method is linked with a possible error relating to the way in which the depolarisation behaviour of the steel is interpreted. Furthermore, it requires techniques to filter out AC in the event of AC interference on the pipeline.
- Measurement of the current density and area specific spread resistance of a probe or coupon to determine the IR-free potential can also be employed. Since AC current is not subject to the same polarisation behaviour as DC, the spread resistance of a defect may be derived from Ohm's law (2) in which the AC voltage and current density are measurable.

  $$U_{AC} = J_{AC}R_S \quad (2)$$

  This allows for the IR-free potential to be determined, via (3), since J_{DC} is also measurable.

  $$E_{IR\text{-}free} = E_{on} - IR = E_{on} - J_{DC}R_S \quad (3)$$

  This method relies on the presence of some AC, and thus for investigating AC corrosion this requirement is not an issue. Essentially, the spread resistance is a frequency-dependent impedance, but at 50/60 Hz the impedance of the double layer capacitance is low, validating the use of (3). [7] [8]

This study uses the relationship between the current density and the spread resistance and the continuous logging of these parameters (using a MetriCorr[i] ICL-02*i* logger) to determine the IR-free potential.

As a baseline for the further discussion; the terms 'polarised potential', 'instant-off potential', 'IR-free potential', 'true surface potential' or other alternative descriptions, can be used interchangeably.

Method

All corrosion experiments in this study were made using 500 µm carbon steel ER probes from MetriCorr[i], having an exposed area of 1 cm^2 with a length/width ratio of 10/1.

pH monitoring under cathodic protection was performed using different pH glass tip electrodes. To account for the steep pH gradient towards the steel surface [4], small electrodes with a tip size of 200 µm (PH-200 from Unisense[ii]) were used (* in Figure 4). These are extremely fragile and broke upon contact with the electrode surface, thus the placement in these experiments was "as close as possible" without risking contact. In addition, a more robust 3 mm tip pH electrode (PHC3359-8 from Radiometer[iii]), shielded on the sides with polymeric shrink sleeve, was brought into contact with the surface. In order to allow for diffusion in and out of the volume, the probe was retracted 100 µm using

[i] MetriCorr, Toerringvej 7, 2610 Roedovre, Denmark
[ii] Unisense, Tueager 1, DK-8200 Aarhus N, Denmark
[iii] Hach, Loveland, CO 80539, US

a micro-manipulator (** in Figure 4). The latter proved more unstable, probably due to gas bubbles momentarily blocking the sensitive surface or a higher sensitivity to electrical noise.

As glass pH electrodes are influenced by electric fields, the experimental setup was equipped with timers disrupting the DC and AC (if any) current in a 10/60 s open/closed sequence. The difference between pH measurements with and without current was significant, i.e. several units of pH at times. The pH electrode was logging every second using a Unisense pH/mV-meter coupled with the Sensor Trace Suite Logger software. During the 10 seconds disruption of current the pH stabilised and a value could be read. The pH electrodes were calibrated both before and after the experiment in pH = 4.01, 7.01 and 10.01 buffer solutions and any drift of the readings during the experiment was compensated for. The experimental setup can be seen in Figure 3. The AC/DC circuit for AC interference and cathodic protection is similar to that used in previous studies. [9] The 3 mm pH electrode was equipped with an internal reference electrode while the 200 µm pH electrode was coupled with an external calomel electrode (SCE).

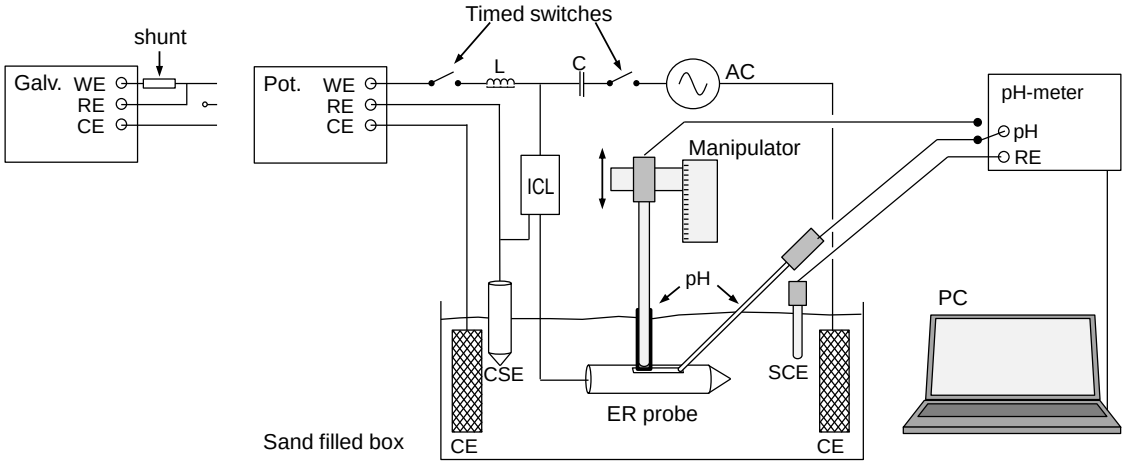

Figure 3: Experimental setup for AC interference of cathodically protected ER probe as well as pH measurement of the protected surface. Cathodic protection in potentio- or galvanostatic setting using a suitable shunt.

All experiments conducted in this study were sand box experiments (0.4 – 0.8mm, quartz sand) with a simulated non-scaling artificial soil solution (NAS) according to Table 1. In some experiments the pH was adjusted by addition of NaOH and measured using a pH electrode. The standard NAS solution mixed with sand has a soil resistivity of 17.3 Ωm and neutral pH_0

Table 1: Non-scaling Artificial Soil (NAS) solution

Species	Concentration
Na_2SO_4	$5.0 \cdot 10^{-3}$ M
$NaHCO_3$	$2.5 \cdot 10^{-3}$ M
NaCl	$10.0 \cdot 10^{-3}$ M

Different approaches were chosen to investigate the high pH dihypoferrite corrosive region. These are outlined in experiment I-III:

I. A pH of 13.5 was achieved by the addition of NaOH to the NAS. Applied AC interference was increased from 1.5 to 5 V. This was done, first at the free corrosion potential (exp. Ia), and secondly polarised with DC to obtain an IR-free potential of -1.11 V_{CSE} on the hydrogen line in the $HFeO_2^-$ region (exp. Ib). Additional measurements were performed at 6,3 V_{AC}.

II. A constant cathodic current of J_{DC} = -30 A/m^2, was introduced, theoretically yielding pH = 12.318 + 0.714·log(30) = 13.4. AC interference was induced and increased from 1-25 V while the IR-free potential and other electrical parameters were logged.

III. A pH = 12 NAS-solution was used and a constant cathodic current of J_{DC} = -0.3 A/m^2 was induced theoretically maintaining the pH = 12.318 + 0.714·log(0.3) = 11.95. AC interference was induced and increased from 1-37 V. while the IR-free potential and other electrical parameters were logged.

In all experiments each AC/DC setting was kept constant for a minimum of two days in order to evaluate corrosion rate on an ER probe.

Results

Monitoring of the steel surface pH under cathodic protection proved very difficult with the given experimental setup and choice of micro pH-electrodes. The results shown in Figure 4a are three readings obtained under varying conditions. In all the experiments under cathodic protection, the measured pH increased quickly to above pH = 11 proceeding to stable levels of pH = 11.95 (J_{DC} = -0.132 A/m^2) and pH = 12.07 (J_{DC} = -1 A/m^2) in the galvanostatic experiments. In an experiment under potential control and overlying AC (-1.5 V_{CSE}, 10 V_{AC}), pH increased to 13.37 at a final J_{DC} = -26.3 A/m^2 (see Figure 5). These results are those included in Figure 2 for comparison with other studies.

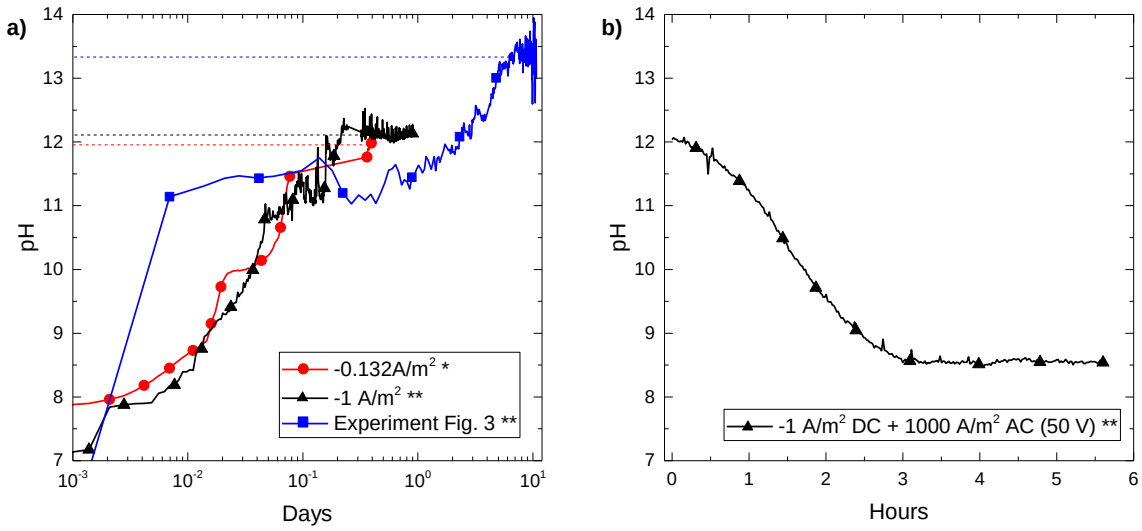

Figure 4: pH evolution over time at various cathodic protection settings. a) Two experiments in galvanostatic setting and one under -1.5 V_{CSE} potential control as shown in Fig. 3 with 10 V AC. b) The effect of high alternating current on pH on the -1 A/m^2 cathodic current probe. (200 µm tip pH glass electrode. ** 3 mm tip pH glass electrode with shielded sides. See Methods.)*

To investigate the influence of AC on the pH of a cathodically protected surface, increasing AC current densities J_{AC} = 10, 35, 100, 230, 500 and 1000 A/m^2 were introduced on the J_{DC} = -1 A/m^2 surface, and held constant for 30 minutes at each level. No effect was visible until 1000 A/m^2 at which point the pH began to decline (Figure 4b). The current density was left at 1000 A/m^2 resulting in the pH declining to neutral pH = 8.5 after 3 hours, despite a constant cathodic current density of -1 A/m^2. This may be explained by consumption of hydroxyl ions (4) during the anodic cycle of AC.

$$4OH^- \rightarrow 2H_2O + O_2 + 4e^- \quad (4)$$

The cathodic cycle of AC is likewise expected to increase the hydroxyl concentration, but differences in the kinetics of the oxygen and hydrogen evolution reactions may explain the overall lowering of pH.

U_{AC} = 50 V alternating voltage was needed to reach the high current density of 1000 A/m^2. This caused depolarisation of the steel to ~-500 mV$_{CSE}$ which is not representative of steel under cathodic protection. As pH reduced to 8.5 and settled, the IR-free potential reduced to ~-770 mV$_{CSE}$, which corresponds well with a point on the hydrogen-line in the Pourbaix diagram at pH = 8.5 (Figure 1).

Figure 5 shows a probe under potential controlled cathodic protection and 15 V AC interference. The potential was kept at -1500 mV$_{CSE}$ for 7 days, after which it was changed to -1000 mV$_{CSE}$.

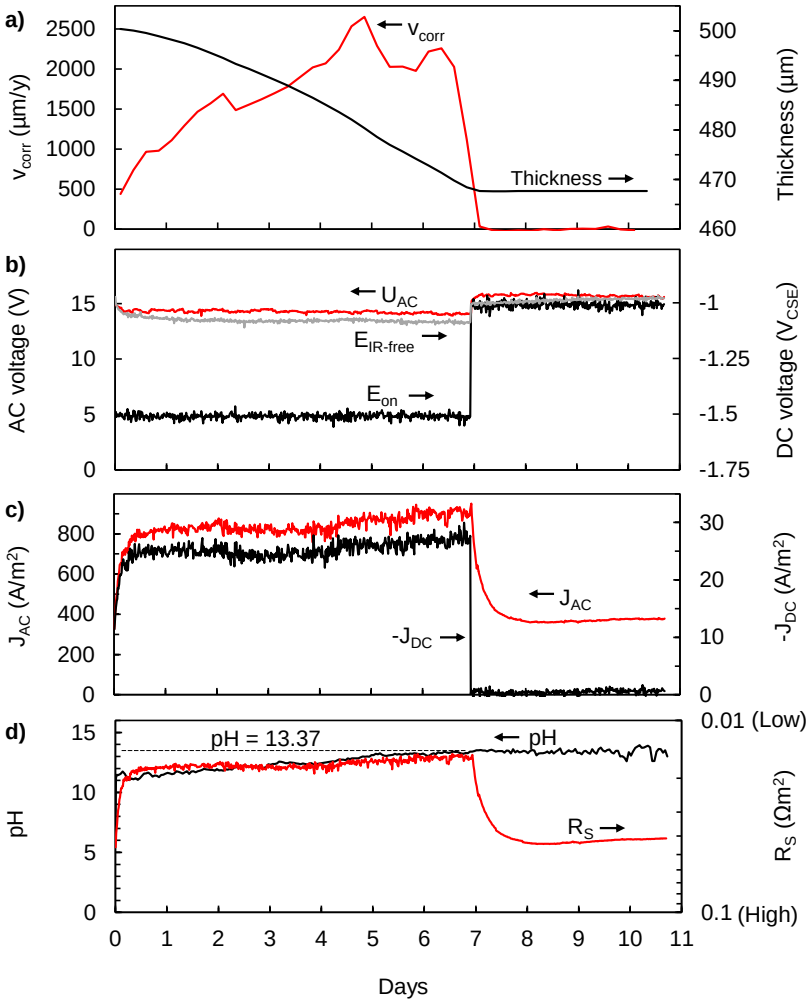

Figure 5: 15 V AC on an ER probe under cathodic protection at first -1500 mV_{CSE} resulting in heavy corrosion, and after 7 days -1000 mV_{CSE} halting AC corrosion. The pH and spread resistance were monitored.

pH was measured using a shielded 3 mm electrode (**). Upon applying CP to the system, the pH immediately rose to pH > 11, thereafter increasing at a much lower rate. Although the change in potential after 7 days resulted in a reduction of the cathodic current to <1 A/m^2, the pH remained high. Lowering of pH relies on diffusion of OH^- ions away from the surface, which is a slow process. However, it is suspected that the actual pH may have changed faster than measured due to the experimental design. There is a possibility of a high response time of the shielded electrode due to the thin crevice on the sides of the pH sensitive glass-sphere. Figure 5d illustrates the commonly recognized relationship between pH and spread resistance. As can be seen, corrosion is immediately stopped upon changing the potential, while the pH remains unchanged. This indicates that that it is not a pH dependent mechanism. A possible explanation of this can be found in the Pourbaix diagram in Figure 1: the IR-free potential in Figure 5b immediately changes from -1100 mV_{CSE} to -1000 mV_{CSE}, which, despite being only a difference of 100 mV, shifts the steel out of the 10^{-4} mol/L stability region of $HFeO_2^-$.

Figure 6 and Figure 7 show corrosion rate data from experiment I-III. The results of these experiments are outlined below:

I. In Figure 6b and Figure 7 it can be seen that no corrosion was recorded when the potential was left under free corrosion conditions (experiment Ia), despite high pH = 13.5 and increasing AC interference. When polarised to -1.11 V_{CSE} (on the hydrogen line in the $HFeO_2^-$ region) (experiment Ib), no corrosion was detected until the level of AC interference was increased. This may be interpreted as disappearance of the high pH corrosion region due to an initial increase of the concentration of $HFeO_2^-$ ions. However, upon increasing AC, these ions are continuously oxidised during anodic polarisation or reduced during cathodic polarisation, thus the $HFeO_2^-$ concentration remains low, stabilising the high pH corrosion

region.
Table 2 shows measured values during experiment Ia and b. The AC current densities were high despite low U_{AC} levels due to the very low spread resistance of the high pH solution.

Table 2: Measured parameters in experiment I

	U_{AC} (V)	E_{ON} (V_{CSE})	$E_{IR\text{-}free}$ (V_{CSE})	J_{AC} (A/m^2)	J_{DC} (A/m^2)	R_S ($m\Omega m^2$)	v_{corr} (µm/yr)
a) "free"	1.6	-0.26	-0.26	399	-0.10	4.0	0
	2.6	-0.25	-0.25	616	-0.09	4.2	0
	3.7	-0.21	-0.21	781	-0.07	4.7	0
	5.2	-0.12	-0.12	484	-0.04	11.4	0
	6.3	-0.82	-0.82	436	-0.03	14.6	0
b) polarised	1.5	-1.11	-1.11	233	-0.2	6.4	0
	2.6	-1.11	-1.11	316	-0.4	8.3	0
	3.6	-1.12	-1.11	542	-1.8	6.6	77
	5.0	-1.13	-1.11	810	-3.5	6.3	294
	6.2	-1.18	-1.11	1138	-13.9	5.5	5215

The non-polarised experiment (Ia) exhibited an increasing spread resistance upon increasing the AC interference, lowering the AC current densities. For the polarised experiment (1b), the artificially maintained pH allowed for high AC corrosion rates at E_{ON}-potentials that are not usually associated with AC corrosion.
Upon increasing the AC interference of the polarised probe, the on-potential necessary to maintain the IR-free potential decreased due to depolarisation while $-J_{DC}$ increased (Table 2). An explanation may lie in de-alkalisation caused during positive AC potential excursions, necessitating an increased cathodic current to maintain high pH and the pre-set IR-free potential.

II. At a galvanostatic cathodic current of J_{DC} = -30 A/m^2 the potential was allowed to float. At zero AC interference, the IR-free potential was as low as -1.5 V_{CSE}, placing the steel in the immune region where no corrosion was measured. Upon increasing the AC interference, the steel de-polarised into the $HFeO_2^-$ stability region. Corrosion rates increased until the IR-free potential passed the 10^{-4} mol/L line at -1.082 V_{CSE} (Figure 6b), above which the corrosion rates again declined (Figure 7). This is difficult to explain using traditional AC corrosion mechanisms [10], but has also been observed in other studies. [11] Pourbaix himself showed that the corrosion rate inside the high pH corrosion region increases towards the upper stability limit (at higher potentials). [1]

III. At pH = 12 and a galvanostatic current of J_{DC} = -0.3 A/m^2, high pH corrosion was not observed. It occurred, instead, at much higher IR-free potentials (above -0.85 V_{CSE}). This experiment is similar to that in Figure 4b (very high AC interference and a small constant cathodic current, but no control of the potential) that showed de-alkalisation, and a subsequent settling of the IR-free potential on the hydrogen line in the low pH corrosion region. The same mechanism is suspected to place the high measured corrosion rates inside the low pH corrosion region, by a projection of the measured IR-free potentials onto the hydrogen line (Figure 6a), provided that the constant cathodic current is due, solely or mainly, to hydrogen evolution, and not reduction of alternative species such as corrosion products. This implies that an IR-free potential more positive than the hydrogen line at a theoretical pH($-J_{DC}$) given by equation (1) may be used as an approximate pH measurement in a galvanostatic CP experiment.

The corrosion rate in experiment Ib was extremely high: >5 mm/yr, measured over 3 days. This is high even for AC corrosion, but perfectly demonstrates the impact of the three factors; an IR-free potential inside the high pH corrosion region, high pH and high AC interference. The circumstances for these conditions to be fulfilled may be very dependent on the chemical system possibly explaining the variation of corrosion rate data in different studies.

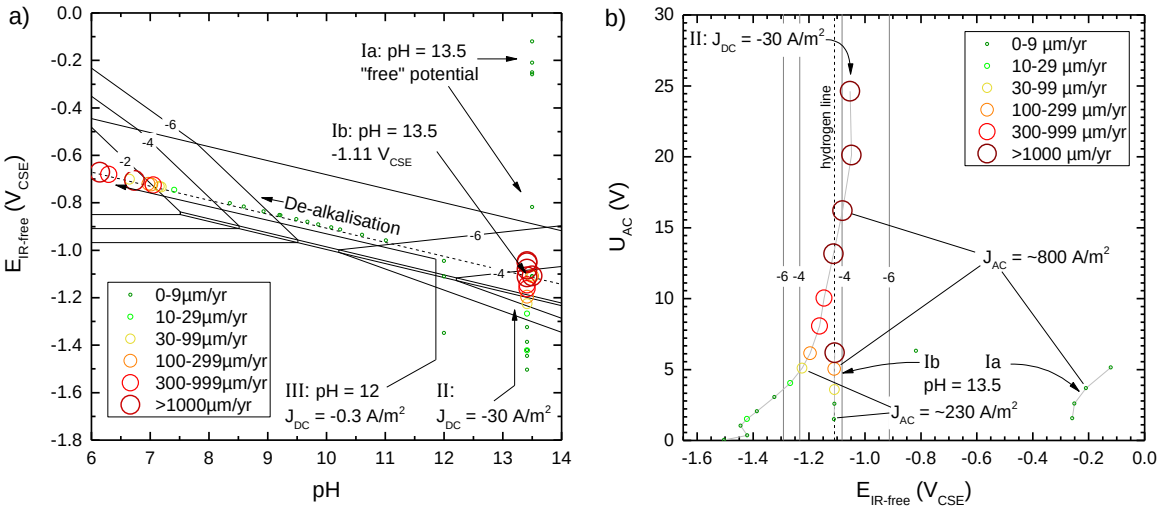

Figure 6: Plot of corrosion rate data from experiments I-III. a) Pourbaix diagram. Exp. I and II illustrate how corrosion is present primarily inside the 10^{-4} mol/L $HFeO_2^-$ area (and not above or below). Corrosion in exp. III can be explained as low pH corrosion by projection of all points above the hydrogen line onto the hydrogen line via de-alkalisation as demonstrated in Figure 4b. b) pH = 13.5 cross-section of the Pourbaix diagram showing the effect of increasing AC: i.e. depolarisation of exp. II and stabilisation of the $HFeO_2^-$ region in exp. Ib.

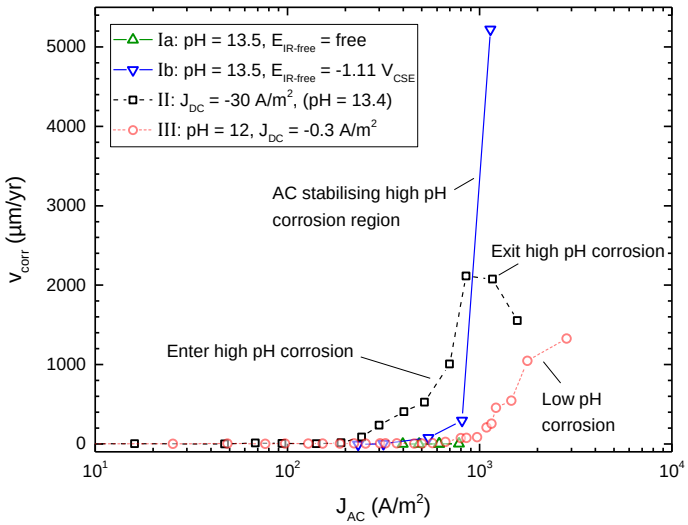

Figure 7: Corrosion rate data from Exp I-III as a function of J_{AC}. Corrosion rate increases in exp. II upon entering the 10^{-4} mol/L $HFeO_2^-$ region, and decreases at higher J_{AC}. Exp. II illustrates how AC stabilises the high pH corrosion region

Processing of previously published data

The correlation between J_{DC} and pH in conjunction with the IR-free potential and the corrosion rate measured from ER probes, allows for mapping of corrosion rates directly in the Pourbaix diagram. Numerous experiments have been carried out in other studies reporting these parameters, but have not previously been presented in this way. Data from specific studies, as referenced, has been treated and is shown in Figure 8. Corrosion rate data measured with ER probes is presented in first the J_{AC}/-J_{DC} plot with indication of the EN15280:2015 criteria ($-J_{DC}$ = -1 A/m², J_{AC} = 30 A/m² and $J_{AC}/-J_{DC}$ < 3). The same corrosion rate data is presented in an adjacent Pourbaix diagram representation based on the IR-free potential and the pH calculated from $-J_{DC}$ using (1). De-alkalisation caused by AC, as demonstrated in Figure 4b, is not suspected to take place in any of the presented data. This effect has only been proven under galvanostatic controlled CP and all of the data presented in Figure 8 are from potentiostatic controlled CP experiments.

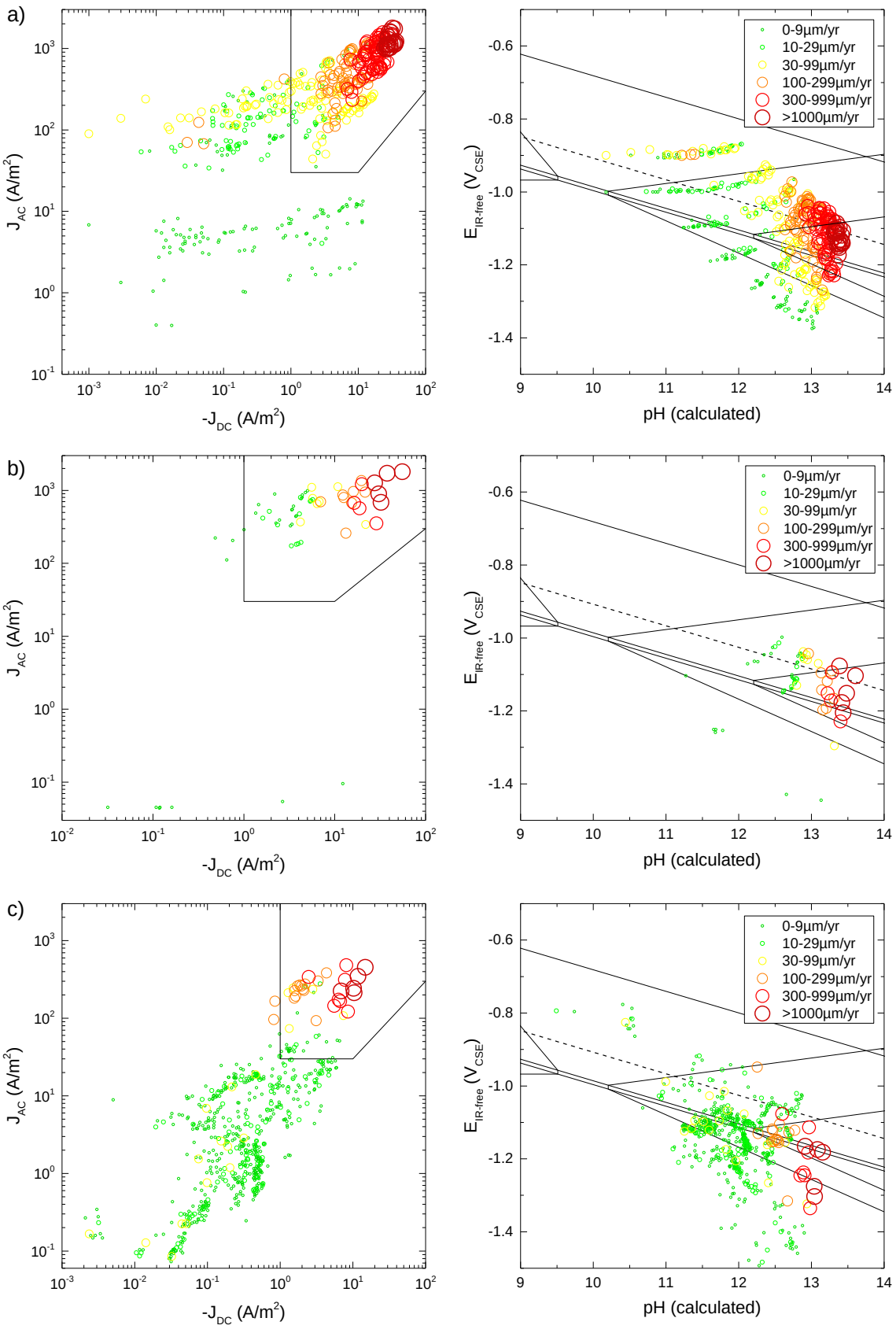
a)
b)
c)
J_{AC} (A/m^2)
$-J_{DC}$ (A/m^2)
$E_{IR\text{-}free}$ (V_{CSE})
pH (calculated)
0-9µm/yr
10-29µm/yr
30-99µm/yr
100-299µm/yr
300-999µm/yr
>1000µm/yr

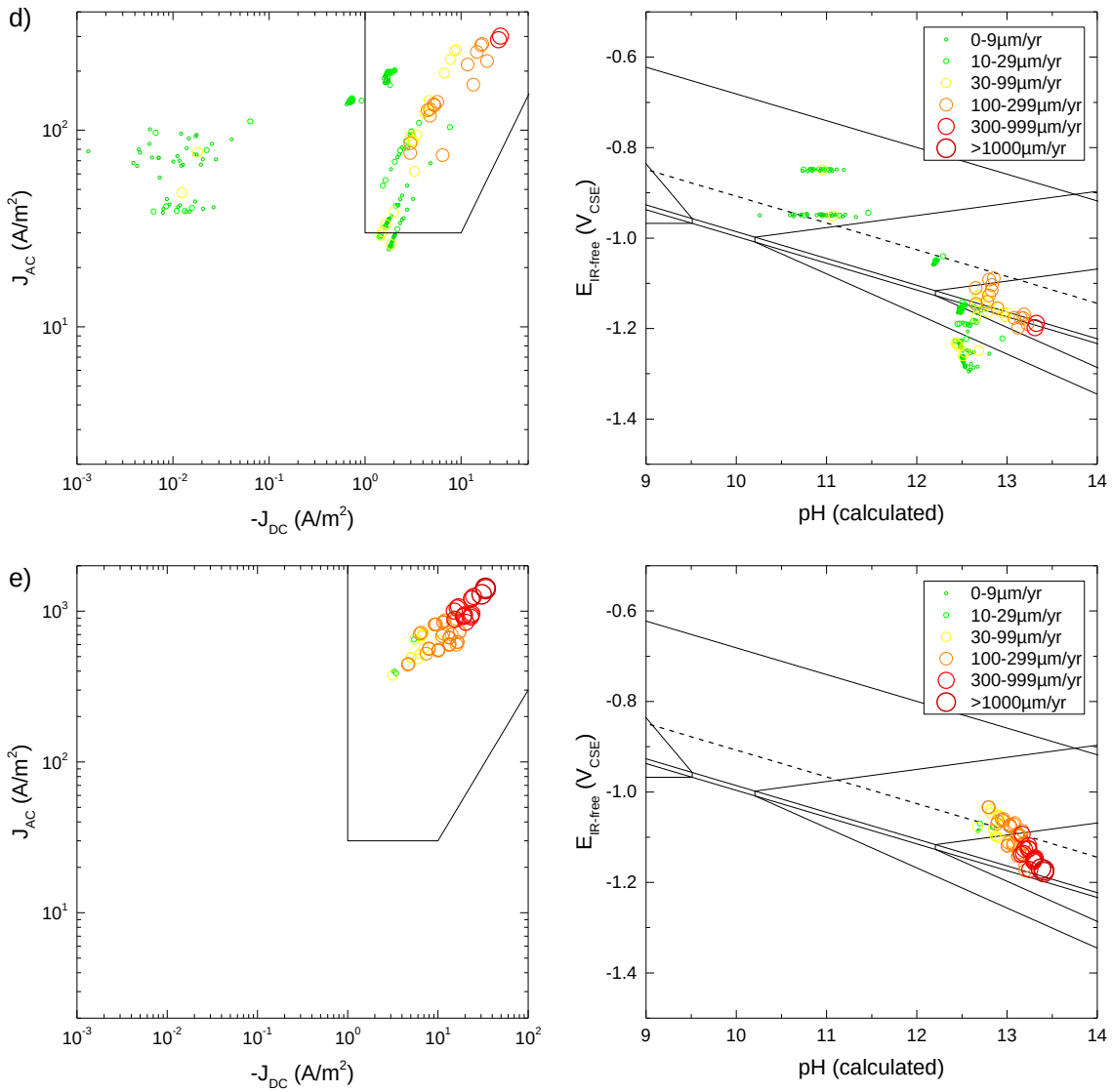

Figure 8: AC/DC current density plot and Pourbaix diagram presentation.
a) Corrosion rate data from various chemical environments. 24 hours per point. [11]
b) Experiments with time-varied AC interference and increasing cathodic polarisation. >1 week per point. [12]
c) Field corrosion rate data from 5 measuring stations on a AC interfered pipeline. 48 hours per point. [11]
d) Corrosion rate data from scaling environment (10V_{AC}, -0.85 - -2.0 V_{CSE}). 24 hours per point. [9]
e) Corrosion rate data from probes with different orientations (20V_{AC}, -1.25 - -1.65 V_{CSE}). 1 week per point. [8]

As was found in experiments I-III, the correlation between high corrosion rates and the 10^{-4} $HFeO_2^-$ region in the Pourbaix diagram is remarkable. One is drawn towards the conclusion that the empirically determined J_{AC} and J_{DC} current density limits simply outline conditions that may bring the steel into the high pH corrosion region. For example, the J_{DC} = -1 A/m^2 limit corresponds to pH = 12.3 using equation (1) and the pH value at which the 10^{-4} $HFeO_2^-$ region begins is pH = 12.2 (using the stated Gibb's free energies in Figure 1).

Discussion

The findings of this simple study imply that a distinction between galvanostatic and potentiostatic cathodic protection is necessary when investigating AC corrosion.

It is generally accepted that the -0.85 V_{CSE} criterion for CP is linked to passivation by alkalisation. [3] This study postulates that depolarisation of a system under galvanostatic CP can be caused by the inverse mechanism; de-alkalisation of the local environment caused by AC, as shown in Figure 4b.

The amount of data presented in this study is insufficient to establish correlations between AC interference, IR-free potential and pH. However, from this study the de-alkalisation appears to be an AC dependent phenomenon, causing a positive shift of the IR-free potential, apparently linked to the hydrogen line when a cathodic current is present.

This observation can prove important to the present understanding AC corrosion under CP. This is due to the fact that a large amount of investigations are based on galvanostatic DC currents because this provides overview of the effect of varying this parameter. [13] However, the information obtained about the influence of AC on the corrosion rate might relate to the low pH corrosion region. This is not comparable to the situation of potential controlled cathodic protection representing the vast majority, if not all of real-life CP systems.

Du et.Al. (2017) carried out a series of galvanostatic tests at DC current densities: J_{DC} = -0.023, -0.3, -1.65 and -18.16 A/m^2 with increasing AC current density J_{AC} = 0, 30, 100, 200 and 300 A/m^2. [13] They found that AC caused a strong depolarisation over 4 days and the effect was more pronounced in the high DC current experiments. In the low DC current density experiments, a maximum potential of ~-0.83 V_{CSE} appeared to be reached at 300 A/m^2 J_{AC}. In the light of the findings in the present study, this may be explained by de-alkalisation. As the DC current is kept constant, ensuring an IR-free potential close to the hydrogen line, this may be interpreted directly as a pH-value. This suggests a correlation between the maximum degree of de-alkalisation, and the J_{AC} and J_{DC} settings.

The above point will most likely also be true for the many studies of AC interference on steel not subject to CP that claim to investigate AC corrosion of pipelines. [14] [15] [16] [17] [18] AC interference of increasing magnitude may cause de-alkalisation and thus low pH corrosion, however this system is fundamentally different to that of steel under cathodic protection.

Potentiostatic CP will be influenced differently by increasing AC interference. In this case, AC depolarisation will cause enhancement of the cathodic current with increasing AC interference (via *faradaic rectification* [2]) causing an increase in pH, as well as a shift of the IR-free potential towards the hydrogen line via lowering of the hydrogen overvoltage. The combined effect may cause the steel to enter the high pH corrosion region.

If the $E_{IR\text{-}free} \leq$ -850 mV_{CSE} criterion is fulfilled, there should theoretically be no chance of low pH corrosion under potentiostatic CP. However, due to a commonly observed shift of steels OCP to <-850 mV_{CSE} with AC interference, the presence of AC may render this criterion insufficient to avoid corrosion. This causes anodic corrosion and should not be confused with effects of de-alkalisation, nor with high pH corrosion. [9] [11]

pH is a common parameter to change in experiments, i.e. using high or neutral pH environments, often under the assumption that this is representative of steel with or without cathodic protection. [15] [10] [19] The findings of experiment I shows that the IR-free potential is significant in terms of placement in the Pourbaix diagram, proving that assumption untrue. In addition, AC seems necessary to stabilise the high pH corrosion region. Studies have been made in which it was tried to provoke AC corrosion in the high pH corrosion region, but it was not found to be significant. [20] The level of AC was low however, and might have been insufficient to provoke corrosion, as was demonstrated in experiment Ib.

The large amount of previously published corrosion rate data presented in Pourbaix diagrams in Figure 8, indicates that the high pH corrosion region plays a fundamental role in the AC corrosion process (at potentiostatic CP). The standard current density criteria (EN15280:2015) may outline the conditions necessary to bring a steel into this region by a combination of depolarisation of the IR-free potential and an increase of pH.

The corrosion regions in the Pourbaix diagram favour corrosion via dissolved ionic species, but observation of corrosion products in AC corrosion cases or experiments is easily explained. As demonstrated in experiment Ib, a potential and pH inside the high pH corrosion region is not sufficient to cause corrosion, but AC interference is necessary initiate corrosion. This suggests that the alternating polarisation continuously oxidises dissolved ions and stabilises the high pH corrosion region. The observation of different oxides in AC corrosion cases may very well be an effect of unintentional aeration of a sample prior to analysis, rather than an indicator of the corrosion mechanism. Reaction (5) illustrates the anodic reaction in which iron is dissolved as dihypoferrite ion.

$$Fe + 3OH^- \rightarrow HFeO_2^- + H_2O + 2e^- \quad (5)$$

Reaction (7) and (8) represents possible anodic reaction routes to magnetite commonly observed in AC corrosion cases: Either directly via (8) or via the chemical reaction to ferrous hydroxide (6). Equation (8) is essentially a combination of equation (6) and (7) as follows: 3·(6) + (7).

$$HFeO_2^- + H^+ \rightarrow Fe(OH)_2 \quad (6)$$

$$3Fe(OH)_2 + 2OH^- \rightarrow Fe_3O_4 + 4H_2O + 2e^- \quad (7)$$

$$3HFeO_2^- + H^+ \rightarrow Fe_3O_4 + 2H_2O + 2e^- \quad (8)$$

Further oxidation of the formed corrosion products may occur via reactions (9) or (10):

$$4Fe_3O_4 + 6H_2O + O_2 \rightarrow 12FeOOH \quad (9)$$

$$4Fe_3O_4 + O_2 \rightarrow 6Fe_2O_3 \quad (10)$$

Despite the fact that the presented mechanism relies on dissolved dihypoferrite ions, it is clear that the corrosion products from AC corrosion cases are not soluble. Both due to continuous oxidation following the AC frequency, but also due to the steep potential and pH gradient towards the steel interface that strongly minimizes the volume at the surface where corrosion products are soluble. Hence corrosion products will accumulate on the surface as commonly observed. [5]

Conclusion

The simple experiments presented herein as well as an illustration of previously published data implies that AC corrosion, and in particular AC corrosion of cathodically protected structures, which has been subject to much controversy in the past decades, may be partially or entirely explained using the Pourbaix diagram. The effect of AC depends on the type of cathodic protection applied.

- It is well known that AC depolarises steel under cathodic protection shifting the IR-free potential positively from the immune region towards the hydrogen line. This is true for both galvano- or potentiostatic control of the CP system. The latter typical of field applications.
- AC enhances the cathodic current density for potentiostatic cathodic protection via faradaic rectification, thus increasing the pH.
- AC is necessary for stabilising the high pH corrosion region. In a stagnant environment such as soil, the concentration of dissolved $HFeO_2^-$ will increase and the high pH corrosion region will disappear, thus not causing progressing corrosion. Increasing AC causes corrosion in the high pH corrosion region, allegedly due to a constant oxidation or reduction of dissolved $HFeO_2^-$, maintaining a low concentration.
- The combined effect of; depolarisation of the IR-free potential, high pH and stabilisation of the $HFeO_2^-$ region, due to AC on cathodically protected steel, causes high corrosion rates in the high pH region in the Pourbaix diagram.
- High levels of AC cause de-alkalisation of steel under galvanostatic CP. Evidence of the phenomenon is presented in this paper, but the available data is in no way sufficient to allow for quantitative comparisons between AC interference and de-alkalisation.
- De-alkalisation caused by AC is a novel finding that calls for a re-evaluation of numerous published papers investigating AC corrosion of pipelines under galvanostatic- or no cathodic protection, since the corrosion mechanism may be fundamentally different to the case of AC corrosion of cathodically protected pipelines under potential control (low pH vs. high pH corrosion).

The presented experiments are simple, and the results show surprisingly good correlation with the thermodynamically calculated Pourbaix diagram. Evaluation of pH is carried out according to simple relations to the cathodic current density. One experiment strongly indicates that depolarisation of steel by AC to an IR-free potential above the hydrogen line at a theoretical pH($-J_{DC}$) may be interpreted as de-alkalisation. In order to further verify the presented mechanism for AC corrosion, a more robust method of pH measurement, than that used in this study, is necessary. Only very recently, suitable pH measurement techniques for cathodic protection uses have been developed. [21]

References

[1] M. Pourbaix, Atlas of Electrochemical Equilibria in Aqueous Solutions, Houston: National Association of Corrosion Engineers, 1974, pp. 307-321.

[2] A. Junker and L. V. Nielsen, “Monitoring of the pH Evolution at a Cathodically Protected Steel Surface Subject to an AC Voltage Perturbation,” in *CEOCOR*, Luxembourg, 2017.

[3] U. Angst, M. Büchler, B. Martin, H.-G. Schöneich, G. Haynes, S. Leeds and F. Kajiyama, “Cathodic protection of soil buried steel pipelines - a critical discussion of protection criteria and threshold values,” *Materials and Corrosion,* vol. 67, no. 11, pp. 1135-1142, 2016.

[4] A. Brenna, M. V. Diamanti, L. Lazzari and M. Ormellese, “A proposal of AC corrosion mechanism in cathodic protection,” in *Tech. Proc. of NSTI Nanotechnology Conference and Expo*, Danville, CA, 2011.

[5] M. Büchler and D. Joos, “Die Wechselstromkorrosionsgeschwindigkeit: Relevante Einflussgrößen sowie deren Bedeutung für die Dauerhaftigkeit von kathodisch geschützten Rohrleitungen,” *Energie Wasser-Praxis,* vol. 4, pp. 54-66, 2016.

[6] L. V. Nielsen and E. S. Diaz, “Coupon Effects on the IR free Potential,” in *CeoCor*, Stratford-upon-Avon, United Kingdom, 2018.

[7] L. Nielsen, “EIS investigation of the Randles Circuit Elements for Carbon Steel Exposed in Artificial Soil Solution,” Technical University of Denmark & DONG Natural Gas, Kgs. Lyngby, Denmark, 2000.

[8] A. Junker and L. Nielsen, “Effect of Coating Defect Geometry and Orientation in AC Corrosion of Buried Pipelines - Laboratory Experiments,” in *CeoCor*, Ljubljana, Slovakia, 2016.

[9] A. Junker, L. V. Nielsen and P. Møller, “Effect of Chemical Environment and pH on AC Corrosion of Cathodically Protected Structures,” in *CORROSION*, New Orleans, 2017.

[10] M. Büchler and H. G. Schöneich, “Investigation of Alternating Current Corrosion of Cathodically Protected Pipelines: Development of a Detection Method, Mitigation Measures, and a Model for the Mechanism,” *Corrosion,* vol. 65, no. 9, pp. 578-586, 2009.

[11] A. Junker, C. Heinrich, L. Nielsen and P. Møller, “Laboratory and Field Investigation of the Effect of the Chemical Environment on AC Corrosion,” in *CORROSION*, Phoenix, Arizona, 2018.

[12] L. V. Nielsen and A. Junker, “The Impact of Fluctuations in AC Interference on the Corrosion Risk,” PRCI, Houston, 2016.

[13] Y. Du, M. Lu, D. Tang and S. Chen, “Researches on the Effects of AC Interference on CP Parameters and AC Corrosion Risk Assessment for Cathodic Protected Carbon Steel,” in *NACE CORROSION*, New Orleans, LA, 2017.

[14] L. W. Wang, X. H. Wang, Z. Y. Cui, Z. Y. Liu, C. W. Du and X. G. Li, “Effect of alternating voltage on corrosion of X80 and X100 steels in a chloride containing solution – Investigated by AC voltammetry technique,” *Corrosion Science,* vol. 86, no. 1, p. 213–222, 2014.

[15] D. Kuang and Y. F. Cheng, “Understand the AC induced pitting corrosion on pipelines in both high pH and neutral pH carbonate/bicarbonate solutions,” *Corrosion Science,* vol. 85, no. 1, pp. 304-

310, 2014.

[16] Z. Jiang, Y. Du, M. Lu, Y. Zhang, D. Tang and L. Dong, “New findings on the factors accelerating AC corrosion of buried pipeline,” *Corrosion Science,* vol. 81, no. 1, pp. 1-10, 2014 .

[17] S. Goidanich, L. Lazzari and M. Ormellese, “AC Corrosion. Part 2 - Factors Influencing Corrosion Rate,” *Corrosion Science,* vol. 52, no. 3, pp. 916-922, 2010.

[18] A. Q. Fu and Y. F. Cheng, “Effects of alternating current on corrosion of a coated pipeline steel in a chloride-containing carbonate/bicarbonate solution,” *Corrosion Science,* vol. 52, no. 1, pp. 612-619, 2010.

[19] D.-Z. Tang, Y.-X. Du, M.-X. Lu, Y. Liang, Z.-T. Jiang and L. Dong, “Effect of pH value on corrosion of carbon steel under an applied alternating current,” *Materials and Corrosion,* vol. 66, no. 12, pp. 1467-1479, 2015.

[20] A. Pourbaix, P. Carpentiers and R. Gregoor, “Detection of AC Corrosion. Interpretation of Instantaneous IR-Free Potential, Current Density and Phase Angle Measurements,” Rapports Technique Cebelcorr, 2002.

[21] Y. Seguí Femenias, U. Angst and B. Elsener, “Monitoring pH in Corrosion Engineering by means of Thermally Produced Iridium Oxide Electrodes,” *Materials and Corrosion,* vol. 69, no. 1, pp. 76-88, 2018.